ADVANCED MATERIALS

www.advmat.de

Scalable Manufacturing of Solderable and Stretchable Physiologic Sensing Systems

*Yun-Soung Kim, Jesse Lu, Benjamin Shih, Armen Gharibans, Zhanan Zou, Kristen Matsuno, Roman Aguilera, Yoonjae Han, Ann Meek, Jianliang Xiao, Michael T. Tolley, and Todd P. Coleman**

Methods for microfabrication of solderable and stretchable sensing systems (S4s) and a scaled production of adhesive-integrated active S4s for health monitoring are presented. S4s' excellent solderability is achieved by the sputter-deposited nickel-vanadium and gold pad metal layers and copper interconnection. The donor substrate, which is modified with "PI islands" to become selectively adhesive for the S4s, allows the heterogeneous devices to be integrated with large-area adhesives for packaging. The feasibility for S4-based health monitoring is demonstrated by developing an S4 integrated with a strain gauge and an onboard optical indication circuit. Owing to S4s' compatibility with the standard printed circuit board assembly processes, a variety of commercially available surface mount chip components, such as the wafer level chip scale packages, chip resistors, and light-emitting diodes, can be reflow-soldered onto S4s without modifications, demonstrating the versatile and modular nature of S4s. Tegaderm-integrated S4 respiration sensors are tested for robustness for cyclic deformation, maximum stretchability, durability, and biocompatibility for multiday wear time. The results of the tests and demonstration of the respiration sensing indicate that the adhesive-integrated S4s can provide end users a way for unobtrusive health monitoring.

Y.-S. Kim, Dr. A. Gharibans, Y. Han, Prof. T. P. Coleman
Department of Bioengineering
University of California, San Diego
9500 Gilman Drive, La Jolla, CA 92093, USA
E-mail: tpcoleman@ucsd.edu

J. Lu, A. Meek
Department of NanoEngineering
University of California, San Diego
9500 Gilman Drive, La Jolla, CA 92093, USA

B. Shih, K. Matsuno, Prof. M. T. Tolley
Department of Mechanical and Aerospace Engineering
University of California, San Diego
9500 Gilman Drive, La Jolla, CA 92093, USA

Z. Zou, Prof. J. Xiao
Department of Mechanical Engineering
University of Colorado Boulder
1111 Engineering Drive, UCB 427, Boulder, CO 80309, USA

R. Aguilera
Department of Electrical and Computer Engineering
University of California, San Diego
9500 Gilman Drive, La Jolla, CA 92093, USA

DOI: 10.1002/adma.201701312

In the last decade, wearable sensors and wireless health monitoring have been transformed from science fiction to reality, with many products and services now commonly available.[1,2] The form factor dependent nature of the devices' design criteria and their inability to adhere to the skin create challenges for indirect sensing of physiologic signals (e.g., heart rate estimation from optical measurements rather than from an electrocardiogram). The technical challenges these products face, such as motion artifacts, poor signal to noise ratio, and need for additional circuits, generate fidelity and energy tradeoffs that are not always satisfactory. Problems such as these contribute to the recent pessimism about how wristbands and related wearables can truly bring forth the changes in healthcare that we have imagined. It is increasingly being realized that there are needs to monitor physiological signals of interest without being compromised by the abovementioned issues, in manners that are unobtrusive and independent of the sensors' form factor. The sensor's measurement reliability and capabilities to directly capture the target physiology are even more critical if the measured data is to be used for diagnosis. Stretchable electronics have the potential to provide such capabilities. For example, in 2011, epidermal electronics developed by Kim et al. demonstrated the feasibility of wireless physiological monitoring using skin-conforming electronics.[3] The extremely thin and stretchable electronic platform addressed the issues rising from non-contact measurements by effectively eliminating the gap betewen electrode and skin. Since then, various research groups around the globe with collective interests in improving human health have introduced numerous variants of skin-wearable systems involving organic, inorganic semiconductors, fluid-filled circuits, die-thinning, and flexible printed circuit boards (PCBs).[4–8] Each of the technologies mentioned here successfully advanced its precedent counterpart by improving specific aspects of the wearable systems, such as wearability, specificity for target biomarkers, and capabilities to wirelessly transfer data and power. However, the common obstacles many of these new systems face is the technical challenges in going

from proof-of-concept to large-scale fabrication in ways that are cost-effective and compatible with existing processes that fully leverage economies of scale.

A few recent reports have addressed the issues of feasibility in manufacturing and cost using "cut-and-paste" methods, or by making use of commodity materials such as the gold leaf and copper tape.[9,10] While these approaches achieve the goal of low-cost manufacturing and fast prototyping, an end-to-end manufacturing solution enabling the full integration of modern active electronic components, which require a multilayer, high precision interconnection system, is yet to be presented. Moreover, as more sensor systems adopt advanced wireless interconnectivity, on-board integrated circuits (ICs), for example, microprocessor, amplifier, wireless power/data transfer, memory, multiplexer, etc., have become indispensable for skin-wearable devices. Demonstration of connecting various small electronic packages to thin copper traces by a soldering process has been demonstrated recently by Kim et al., but the solderability between chip components and thin, flexible pad systems as well as a strategy for large-scale manufacturing have yet to be established.[11]

Fortunately, over the past decade, advancements in microfabrication processes and flip chip technology—chip assembly method where the active ICs face down to the substrate—have steadily increased the density of input and output connections while decreasing the overall size.[12] With the consistent demand from the mobile phone and wearable device industries, the total flip chip market is expected to reach $35 billion in 2018.[13] Naturally, the majority of chip manufacturers are offering more compact forms of packaging, such as the wafer level chip scale package (WLCSP). Owing to their small form factor (hundreds of microns in thickness and millimeters wide), most WLCSPs, along with other thick film passive components, are good candidates for skin-wearable devices—provided solder-compatible pad system is present in the stretchable substrate.

Within the context of health monitoring, multiple considerations must also be taken into account for packaging such heterogeneous systems including: 1) circuit isolation, 2) ease of application, 3) durability, and 4) biocompatibility with the epidermis. Commercial soft adhesive film dressing (Tegaderm, 3M, USA), for example, can serve as a material to help satisfy these requirements, since its semi-permeable nature provides a good barrier for the underlying electronics, and it is considered one of the clinical-standard film dressings.[14,15] Moreover, the adhesiveness of Tegaderm can be utilized to directly peel completed stretchable devices off of a donor substrate effectively allowing the end users to only remove the liner before use.[16] Finally, the adhesive nature of the system allows the sensors to be applied at desired locations determined by the applications, rather than, for example, to a wrist.

In this report, we present a modularized manufacturing process consisting of four standard manufacturing methods: (a) microfabrication of thin-film interconnection, (b) film transfer using thermal release tape, (c) PCB assembly, and (d) roll packaging. Unlike many previous manufacturing methods that require unconventional usage of equipment or manual dexterity, our method allows the use of standard materials and equipment under each of the four categories and combines their key benefits to enable scalable manufacturing of stretchable electronics.[17–19] The microfabrication steps yield a solderable and stretchable sensing system (S4), which is unique in its compatibility with the standard processes for lead-free PCB assembly, such as the reflow soldering (a high temperature process reaching a maximum of 260 °C), stencil printing of solder paste, and automatic placement of surface mount components. Another novelty, in terms of packaging methods, is in how the presented approach allows scaled integration of heterogeneous electronic systems with large area soft adhesives; this is accomplished by selectively weakening the adhesion of chip components to the donor substrate.

We also provide an exemplar circuit pertaining to human respiratory monitoring with a strain gauge and amplification circuit. In this regard, we characterize its system level behavior and reliability with the use of a soft robotic actuation system that closely mimics abdominal expansion and retraction mechanics. A viability test for health monitoring using the S4 respiration sensor manufactured by the proposed processes is conducted by comparing the accuracy of respiratory rate measurements to that measured simultaneously by a conventional chest strap device. Finally, we investigate the durability and biocompatibility of the S4 by monitoring the functionality and conditions of the sensor and the skin over a period of 72 h.

Manufacturing of S4 Respiration Sensor: **Figure 1**a–d schematically illustrates the four representative processes used to construct an active S4 respiration sensor, and Figure 1e,f shows the exploded view rendering of the device components and application of the sensor on skin, respectively. The details of each process are as follows:

(a) Microfabrication of S4

Conventional IC microfabrication techniques such as spin coating, sputter deposition, chemical vapor deposition, wet/dry etching, and photolithography were used to form the conducting traces, solder pads, and insulative polyimide (PI) layers, shapes of which are specified in computer aided design software (AutoCAD, Autodesk Inc., USA).In order to leverage the benefits of the high manufacturing yield and excellent transferability, all microfabrication steps were carried out on a weakly adhering poly(dimethylsiloxane) (PDMS)-coated substrate (primary donor substrate) as demonstrated by Kang et al.[16] The fully continuous mesh network in the circuit area prevented the localization of stresses caused by epidermal strain, and served as the pathway for the conductive traces (Figure S1, Supporting Information). Device footprint and interconnect lengths were minimized by overlapping multiple copper traces in the same section of the polymer body at different depths, and the design rule of the horseshoe shaped interconnects were guided by previously reported stretchable systems.[20,21]

(b) Transfer of S4 from primary to secondary donor substrate

The completed S4 was peeled-off from the primary donor substrate and onto a thermal release tape (Revalpha 3195M, Nitto Denko, Japan). The thermal release tape containing the S4 was brought into contact with the secondary donor substrate, which is a PDMS-coated substrate patterned with "PI islands", which are additive PI features that render target areas of the secondary donor substrate non-adhesive. Using optical microscope and alignment marks present on both

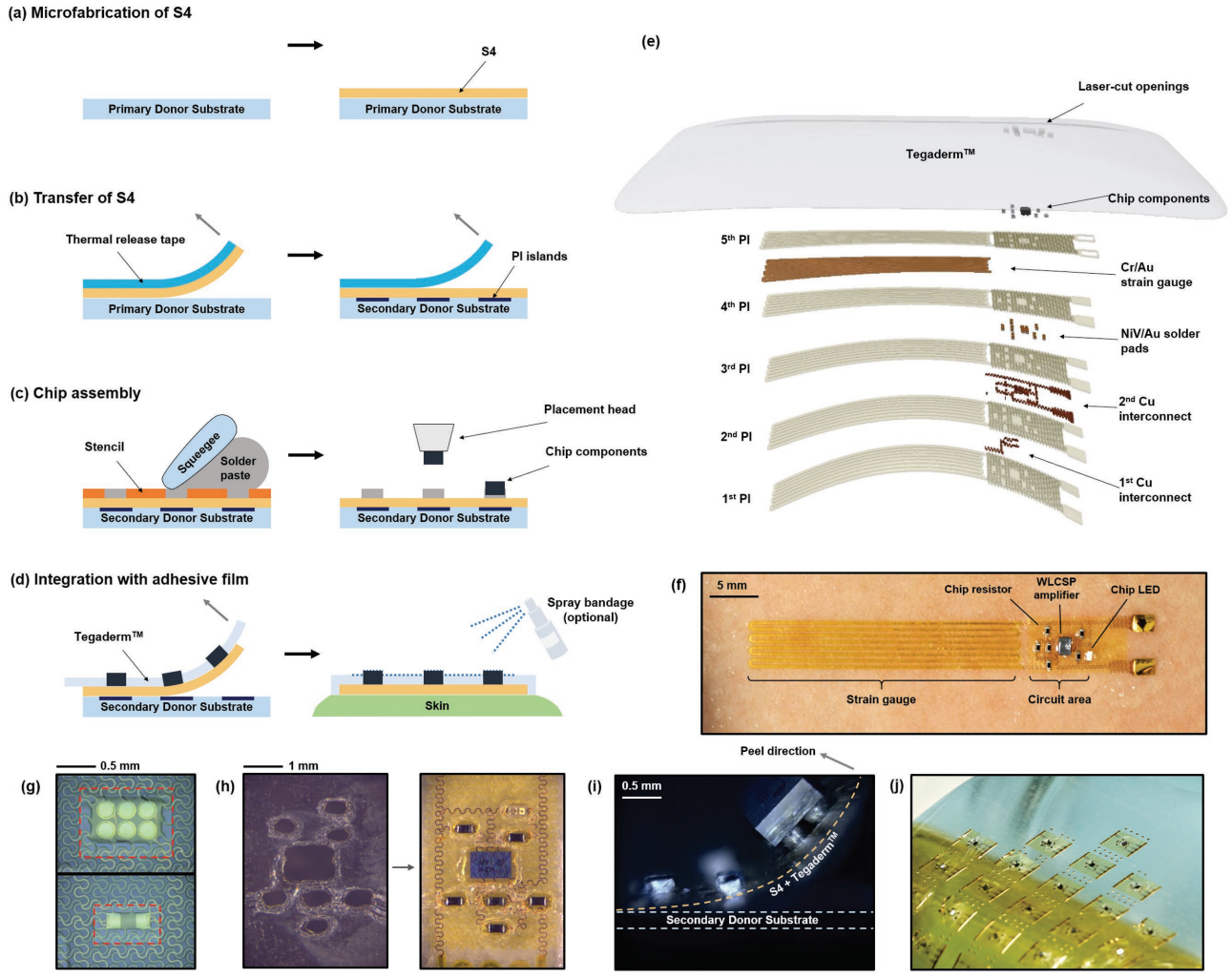

Figure 1. Panels (a)–(d) schematically illustrate the four processes each with its representative steps. a) S4 is constructed on a PDMS-coated primary donor substrate through microfabrication steps. b) Completed S4 is transferred from the primary to secondary donor substrate, a PDMS-coated substrate containing 'PI islands', using a thermal release tape. c) Solder paste is applied by the stencil printing method. The stencil, a 125 µm thick Kapton film with dry-etched openings, is laminated over the donor substrate containing the S4 then the solder paste is dispensed. Swiping across the stencil with a rubber squeegee and releasing the stencil results in printed solder masses only on the surface of the solder pads. Surface mount components are then placed using a three-axis aligner. d) Reflow-soldered S4 is embedded into a target adhesive (e.g., Tegaderm) where laser-etched openings in the adhesive allow it to fully contact with S4. e) Rendering showing the exploded view of the S4 respiration sensor. f) Photograph of the Tegaderm-integrated S4 respiration sensor applied on skin. The circuit is further insulated by the applications of a spray-on-bandage. g) Optical images showing the solderable areas of the 6-Ball WLCSP (top) and the chip resistor (bottom) of the S4 resting on top of 'PI islands' (highlighted). h) Optical images of a laser-etched Tegaderm (left) and a Tegaderm-integrated S4 (right). i) Optical images showing the side view of the S4, chips, and Tegaderm at the instance of peel-off from the secondary donor substrate. j) Photograph showing the large-scale integration of an array of S4 electronics into a large-area Tegaderm. The secondary donor substrate in this case is a sheet of PDMS-coated Kapton (25 µm) wrapped around a cylinder roll.

the S4 and the secondary donor substrate, regions of the S4 containing solder pads were positioned precisely over 'PI islands'. The thermal release tape was released by heating at 120 °C on a hot plate, leaving only the S4 on the secondary donor substrate (Figure 1g).

(c) Chip assembly with reflow soldering

A flexible stencil, made by oxygen plasma etching a 125 µm thick Kapton film, was laminated over the secondary donor substrate and S4. The solder paste (SMD291SNL10T5, Chip Quik, Canada), which is a SAC305 alloy (Sn96.5/Ag3.0/Cu0.5) with an average solder sphere radius of 20 µm, was dispensed over the stencil. Then, a rubber squeegee was swiped across. Removal of the stencil left solder masses to be printed only on desired solder pads on the S4. The chip components were placed onto the designated locations using a three-axis aligner while, the placement accuracy and polarity were maintained with an optical microscope. Recommended reflow temperature profile was followed by placing the substrate on a programmable hot plate.[22]

(d) Integration with soft adhesive films

Once all chip components were soldered onto S4, Tegaderm with openings precisely etched in the shape of chip

components with a CO_2 laser cutting machine (Rabbit RL-80-1290, Rabbit Laser USA, USA) was laminated over the S4 (Figure 1h). After ensuring all chip components had passed through the openings and the S4 was fully in contact with the adhesive film, the Tegaderm was peeled off the secondary donor substrate (Figure 1i). The Tegaderm containing the S4 device was applied on the skin, followed by an optional application of spray-on-bandage (Nexcare, 3M, USA) for total insulation of the chip components from the environment. Finally, we further demonstrated the process's compatibility for large-scale manufacturing by integrating an array of devices with a single large sheet of adhesive. An array of twenty-three amplification circuits was assembled on a secondary donor substrate in a flexible roll format, then integrated into a single large sheet of Tegaderm (15 cm × 20 cm, Figure 1j).

Solderability of S4s: The electrical connection between S4s and surface mount components is made by reflow soldering using solder paste. The paste form of solder provides not only good electrical and thermal conductivity, but its ability to deform to any surface features makes it the most practical solder option for roll-to-roll processes. We specifically chose SAC305 paste for solder connection in order to verify the solderability of S4s with lead-free solder balls, which have become the norm in WLCSP.[23,24] The paste of choice showed efficient transfer of mass during stencil application and resulted in complete and confined wetting of the exposed pads (**Figure 2**a,b). The S4's solder pad design criteria directly employed the industry's standard guidelines. For example, the dimensions of the land patterns and solder paste stencil were determined by the manufacturers' guidelines and by those described by the Association Connecting Electronics Industries (IPC). In regard to IPC-guided land patterns and solder paste stencils, guidelines IPC-SM-782 and IPC-7351 were used, respectively (Figure S2, Supporting Information). Figure 2c shows the planar and cross-sectional dimensions of the land areas for the WLCSP amplifier chip and 0201 type chip resistors. Here, the layers of the spin coated PI are serving as the structural supports for the device, insulator for the multilayered interconnections, and solder mask that retains reflowing solder. Sputter-deposited copper (≈100 nm thick) was used as the interconnection metal due to its resistance to solder as well as good adhesion to oxygen plasma treated PI film.[25] Eliminating the need for an adhesion metal layer, such as chromium or titanium, prevents potential interconnection damage caused by flux component of the solder paste reacting with oxidized adhesion metal layer (Figure S3, Supporting Information). The bond pad metal system is a sputter-deposited bilayer of underlying nickel-vanadium (50 nm, Ni/V, 93/7 wt%), which acts as the anchoring layer for solder, and top gold layer (600 nm), which provides stability during high temperature processes as well, as storage.[26] When the recommended reflow temperature profile was followed, all of WLCSP's solder balls coalesced with printed solder paste and collapsed efficiently onto respective pads (Figure 2d, left). Similarly, the solder at both ends of the chip resistor wet the surface of the metal terminals as well as the pads, effectively fixing the resistor to S4 (Figure 2d, middle). The result of an x-ray inspection also showed that a 68-Ball WLCSP with the same solder ball pitch as in the amplifier chip was free of voids and shorts when the same reflow soldering process was performed (Figure 2d, right).

Strain Gauge, Wheatstone Bridge, and Amplification Circuit: The strain gauge in the S4 respiration sensor is a single-element gauge made of eight parallel Cr/Au (3 nm/6 nm) traces fully insulated with PI, all of which are integrated with Tegaderm. The resulting resistance was 14.1 kΩ ±1%, where the device-to-device variation originated from inherent laboratory variables such as the manual wet etching and photolithography steps. Controlled strain was applied to the gauges by fixing two opposite ends of Tegaderm to a screw-driven manipulator while the displacement was measured using a USB microscope (Dino-Lite, AnMo Electronics Corp., Taiwan) using built-in software. Resistance values were recorded by wiring two ends of the strain gauge directly to an ohmmeter, and the gauge factor ($GF = (\Delta R/R)/\varepsilon$) of the strain gauge was calculated to be ≈1.2, which is typical for thin metal film based strain gauges, but far less than that of single crystalline silicon nanoribbon (43), carbon fiber composite (155), or ZnO wire (1250, **Figure 3**a and Figure S4, Supporting Information).[16,27–29] As such, when integrated into a Wheatstone bridge circuit, the maximum change in voltage was only ≈15 mV (Figure 3b). However, when a stage of a differential amplification was added, the maximum output voltage signal was roughly 3000 mV, which was sufficient to drive the circuit with clear on/off states for the LED (Figure 3c,d). More importantly, since the strain gauge was made with the same set of microfabrication steps required for processing the interconnection system, no sophisticated, cost-prohibitive processes described in the above reports were necessary. The particular choice of the resistor values for three fixed arms of the Wheatstone bridge—namely 14.3 kΩ and two 1 kΩs—was determined by a circuit simulation where it resulted in more distinct on/off states for the LED while reducing the overall current consumed by the circuit (Figure S5, Supporting Information). The 14.3 kΩ resistor was selected in order to illuminate the LED at strain of ≈1%, which is approximately the average epidermal strain at umbilical level observed in adult men during quiet breathing.[30] As a result, with a thin battery connected, the S4 respiration senor reliably detected a user's respiration rate when applied next to the user's umbilicus. (Movie S1 and S2, Supporting Information)

Mechanical Roles of Soft Adhesive Film: One of the most important requirements for stretchable electronics systems that are intended for interfacing with biological tissues is the robustness of the device throughout the cycles of stretching and relaxation. The role of the Tegaderm layer in the presented method was to provide not only an efficient way to 'peel-and-stick' devices to skin, but also to minimize the potential localization of stresses within thin serpentine structures. Simulation of the interconnection layer positioned between skin and Tegaderm using finite element analysis (FEA) revealed a slight reduction (≈10%) in the maximum principal strain in serpentine copper traces bounded closely by non-stretchable components, with maximum strain reaching 8.8×10^{-3} when a bi-axial strain of 1.08% was applied (**Figure 4**a). The strain values observed in the copper interconnection system were much smaller than thin film copper's yield strain, thus the possibility of the interconnection failure due to stress cycles from natural

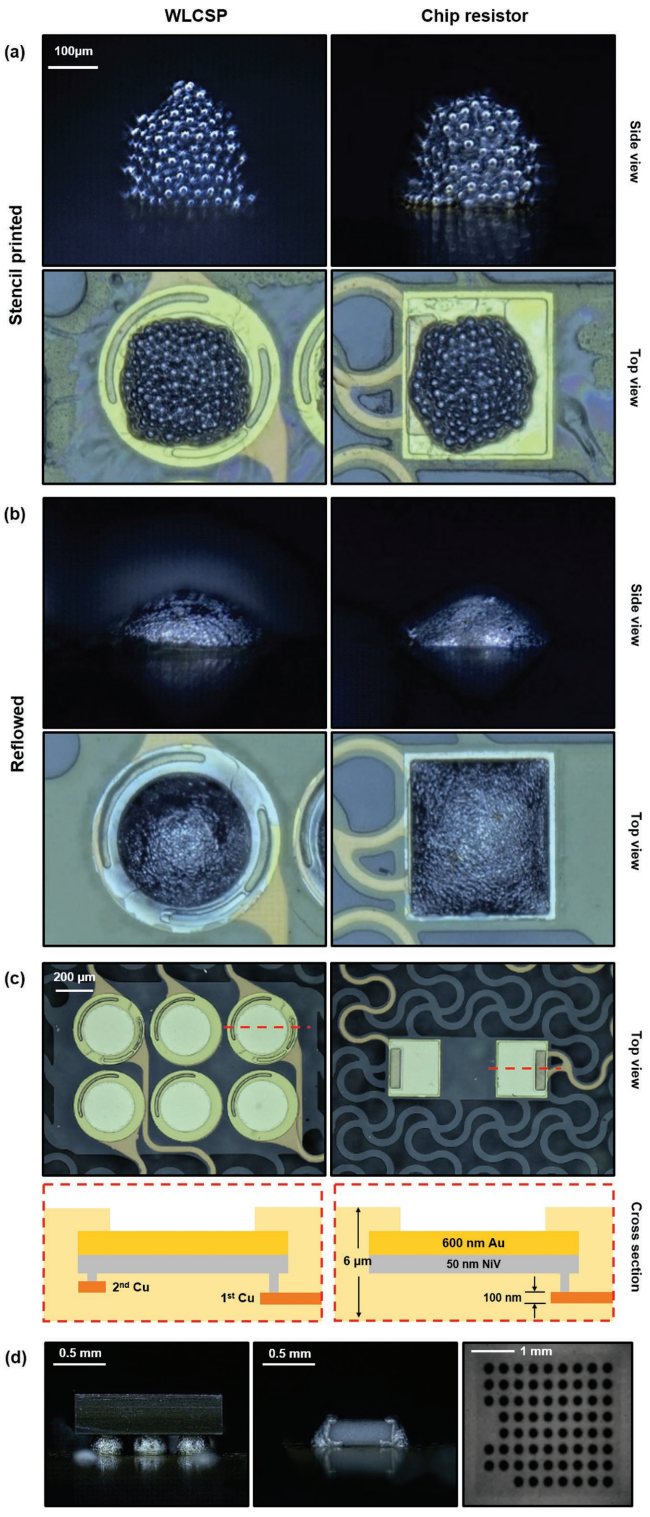

Figure 2. Results of the solderability tests on S4s. a) Optical images of the printed solder mass on a solder pad for WLCSP (left column) and chip resistor (right column). b) Optical images of the reflowed solder on a solder pad for WLCSP (left column) and chip resistor (right column). c) Top row optical images show the layout of the solder pads for the 6-Ball WLCSP (left) and the chip resistor (right) components. Red dotted lines correspond to the respective cross-sectional diagrams directly below. Bottom row diagrams describe the construction of Cu interconnection, vertical interconnect access (via), and NiV/Au solder pad system. d) Optical images showing the result of reflow soldering for a WLCSP amplifier (left) and a chip resistor (middle). Result of an X-ray inspection on a reflow-soldered 68-Ball WLCSP package is free of voids and shorts (right).

breathing is negligible.[31] While the overall stretchability of S4's interconnection system was achieved by extending individual horseshoe shaped features and allowing the out-of-plane deformation, the presence of the overlaid Tegaderm prevented stress localization and provided stability during deformation. This result was in accordance with the result by Lee et al. where moderately thick PI layers promote globally distributed buckling and surrounding low modulus layers—namely skin and Tegaderm—allow for controlled out-of-plane bending for the interconnection.[32] Similar phenomenon of reduction in stress and its localization was found in the strain gauge where excess localization of stress occurred at the center of the gauge in the absence of Tegaderm. The FEA results showed that the presence of Tegaderm helped to distribute strain uniformly across the entire length of the gauge and lowered the maximum strain experienced by the gauge by 46% (Figure 4b). Therefore, the Tegaderm-integrated strain gauge should not only have a lower possibility of failure due to stress localization, but is also a more efficient sensor, as it utilizes the full length of the gauge.

Stretchability of S4s: Following the same layer information used in the FEA (Figure 4c), five S4 devices for each of the amplifier circuit (Figure 4d, top) and the 68-Ball WLCSP chip (Figure 4d, bottom) were assembled to test the maximum stretchability of S4s. The integrity of the solder joints and the interconnection traces during the application of strain was checked by probing pairs of the exposed pads, across which were known resistance values. An abrupt increase in the resistance or out-of-range measurements would indicate a failure in the connectivity along the electrical path between the two test pads. For 68-Ball WLCSP devices, dedicated test pads for each of the 68 pins were allocated along the perimeter of the layout, and probing a combination of two pads would reveal the location of potential disconnect in the respective solder joints or the copper traces at each strain (Figure S6a, Supporting Information). The result of the experiment revealed that all ten S4s' electrical connectivity was robust even up to 40% indicated by the consistency in the resistance values. However, the limiting factor in the stretchability of S4s was found in Tegaderm, which began to exhibit plastic deformation at ≈20% along the boundaries of the laser-etched openings. When strain greater than 20% was applied, the rate of Tegaderm's failure accelerated and delamination of serpentine interconnections around the openings could be observed. It should be noted that the failure of Tegaderm at strains greater than 20% is a natural phenomenon as the polyurethane sheet is expected to exhibit a plastic deformation profile after 15% strain.[33] Therefore, while the serpentine interconnection system and the solder joints could withstand strain exceeding 40%, the effective maximum stretchability of S4s is considered to be 15% due to the limitation in the particular choice of the soft adhesive film. While the maximum stretchability of 15% may be smaller compared to some stretchable interconnection platforms, it is within the physiological relevance. In other words, most parts of human skin do not exhibit strain higher than 15%, and the physiologic

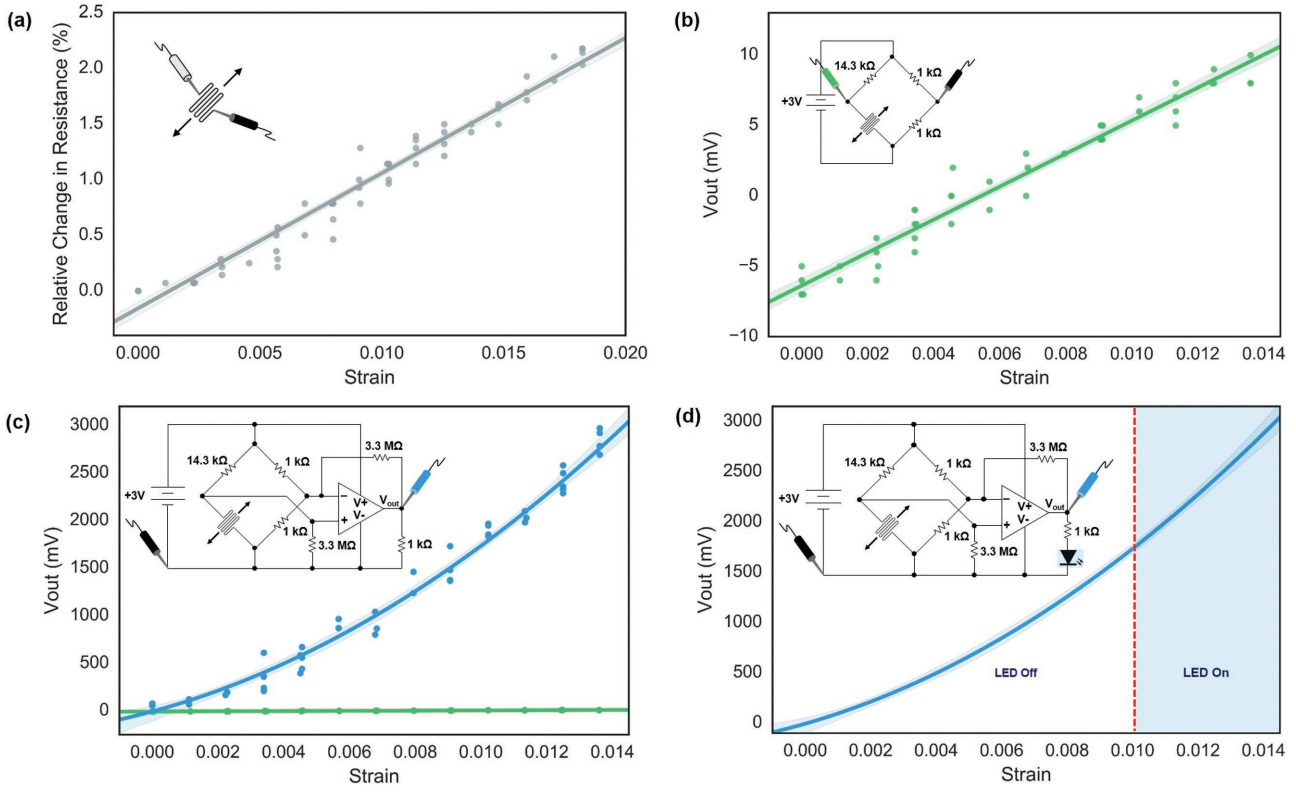

Figure 3. a) Relative change in resistance versus strain for a Tegaderm-integrated strain gauge. Linear least-squares regression of all measurement points (R^2 = 0.98, p = 3.8e−45, order = 1) is used to calculate the gauge factor (≈1.2). (b) Output of the Wheatstone bridge circuit versus strain (R^2 = 0.98, p = 1.9e-32, order = 1). A 14.1 kΩ Tegaderm-integrated strain gauge, and a 14.3 kΩ and two 1 kΩ chip resistors make up the four bridge arms. c) Output of the amplified Wheatstone bridge circuit versus strain (R^2 = 0.98, p = 3.8e-45, order = 2, blue plot). d) Circuit operation for the respiration sensing. Red dashed line represents the threshold strain for LED illumination.

limitation is measured to be ≈45% in areas such as the fully flexed knee or elbow.[34] Consequently, the electrical robustness of S4s was verified within the bounds of natural stretching of skin, and the placement of larger components should avoid the joint areas in such demanding cases.

Automatic Cyclic Loading on S4s Using a Human Surrogate System: Since S4s were intended to interface the mechanically dynamic human skin with constant deformation, an investigation into the mechanical and electrical robustness under intended physiological environment was necessary. In order to verify the robustness of the S4 respiration sensors, we devised a human surrogate system, which would provide a controlled platform for devices to be examined with controlled variables without involving human factors. This system, a pneumatically actuated soft actuator, was designed to uniformly expand and retract radially to replicate the abdominal expansion/retraction due to breathing, capturing the continuous behavior of the attached devices, not just at the static "strained" vs "un-strained" states. The S4 respiration sensor is consists of two parts from a structural stand point: the strain gauge, which is designed to reliably and consistently detect the strain, and the amplifier circuit, which is designed to consistently perform throughout the cyclic deformation. As such, we examined the two parts separately. Figure S7 and Movie S3 in the Supporting Information show the details of the experiment setup and the characteristics of the actuator.

(a) Robustness of the Tegaderm-integrated strain gauge

Figure 4f shows three 20 s windows of data from the beginning, middle, and end of a 3 h recording, where the high fidelity between the two data can be visibly observed. Also, the linear least-squares regression (R = 0.96, p < 0.001) for the entire recording quantitatively verifies that the responsiveness of the Tegaderm-integrated strain gauge to the motion of the actuator showed no sign of degradation over time, suggesting the two plots are statistically commensurate for the total 3 h testing duration.

(b) Robustness of the Tegaderm-integrated S4 amplifier circuit

Figure 4h describes the result of the 3 h cyclic loading test on the amplifier circuit where the linear least-squares regression (R = 0.98, p < 0.001) reveals that the measured output of the amplifier circuit is consistently and highly correlated with the input signal. The three 5 s windows of data from the beginning, middle, and end of a 3 h recording demonstrate that the electrical function of the amplifier circuit in the form of S4 is unaffected by the continuous mechanical disturbance. The higher correlation value from the amplifier circuit data compared to that from the strain gauge test points to the built-in function of the amplifier chip to reject common-mode noise and the possible distortion introduced in the process of converting color markers' positions into

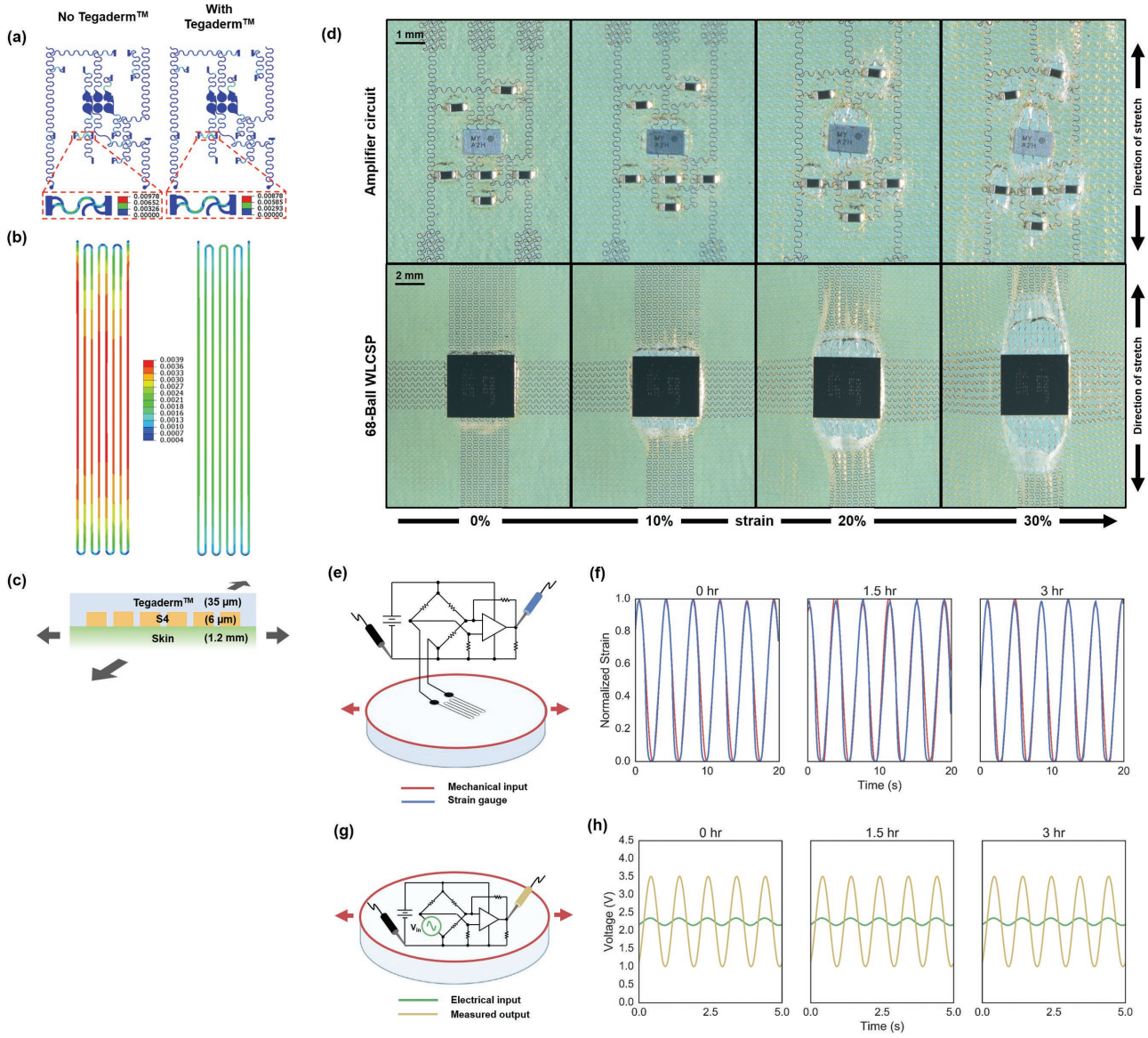

Figure 4. a) FEA result indicates a reduction in the maximum principal strain in the Cu interconnection from 9.8×10^{-3} to 8.8×10^{-3} under a biaxial strain of 1.08% when Tegaderm is integrated with S4 amplifier circuit. b) Under the same condition, the Tegaderm-integrated strain gauge experiences a significant reduction in the maximum principal strain (from 3.9×10^{-3} to 2.2×10^{-3}) as well as the more uniform distribution of the strain across the gauge when it is integrated with Tegaderm. c) Schematic illustration of the simulation conditions. The S4 layer (thickness: 6 μm) is constrained by the top Tegaderm layer (Young's modulus: 1.2 MPa, thickness: 35 μm) and the bottom skin layer (Young's modulus: 0.42 MPa, thickness: 1.2 mm, incompressible). The arrows represent the 1.08% biaxial strain. d) Optical photographs of the S4s under various strains from 0% to 30% for the amplifier circuit (top row) and the 68-Ball WLCSP chip (bottom row). e) Schematic illustration of the cyclic loading test of the strain gauge. Only the Tegaderm-integrated strain gauge undergoes the cyclic deformation. (f) The plots show three 20 s windows of the actuator strain (red) and the strain gauge output (blue) from the beginning (left), middle (middle), and last (right) of the 3 h test. The Tegaderm-integrated strain gauge shows consistency in its responsiveness to cyclic loading throughout the test. g) Schematic illustration of the cyclic loading test of the amplifier circuit where the strain gauge is replaced with a sine voltage wave (green). Here, the actuation scheme is the same as in panel (e) and the electrical output (yellow) is the measured circuit output. h) The plots show three 5 s windows of the electrical input signal (green) and the measured circuit output (yellow) revealing the consistency in the amplifier's performance over the 3 h test.

strain values. Nonetheless, the result of the cyclic test proved the presented scheme of S4's interconnection system provided the reliable connectivity among the multiple resistors and the amplifier. This suggests that the sensing and electrical functionalities of S4s can sustain throughout cyclic deformation.

Finally, the human surrogate system allowed us to investigate the long-term responses of the stretchable electronics to specific human anatomical movements without involving human subjects. For example, multiple difficulties and uncertainties (i.e., subject incompliance and variations in physical/medical conditions) could arise if multi-hour tests were to be conducted

using human volunteers. Using 3D printing technology, silicone molding techniques, and the actuation method described in this report, a variety of anatomies and medical conditions (e.g., asthma, sleep apnea) could be created, with deformation schemes that closely replicate those of human counterparts.

Validity Testing of S4 Respiration Sensor Using a Chest Strap System: In order to determine the validity of the S4 respiration sensor in measuring the respiratory rate, the LED illumination pattern of the adhesive-integrated system was compared to the raw respiratory data obtained by the BioHarness 3 (Zephyr Technology Corporation, USA), an FDA-approved chest strap device that measures the expansion and retraction of the thoracic cage. With the Zephyr device strapped to the chest and the S4 sensor simultaneously attached at the umbilical level, the subject was instructed to breathe naturally for 3 min (**Figure 5**a,b). In order to determine the on–off timing of the LED from the sensor, we extracted each frame of the recorded video and synchronized to the data transmitted by the Zephyr's Bluetooth module. Figure 5c illustrates the temporal agreement between the two measurements such that the time when LED is on (shaded light blue) corresponds with every local maximum of the chest strain measured by the strap. A noteworthy finding from the comparison of the two datasets is that the responsiveness of the illumination is independent of the baseline fluctuation in the strain recorded by the chest strap. One explanation to this finding may be that breathing is naturally a two-component behavior consisting of abdominal and thoracic breathing, and depending on the person's body position and wakefulness, the ratio of the two can vary.[35,36] In fact, this result points to the potential of S4-based health monitoring and diagnosis where the clinicians can gain new insights from multipoint physiological recordings by simply attaching adhesive-integrated electronics over both the abdominal and thoracic cavities.[37] Finally, the S4 respiration sensor was proven to be a valid alternative for measuring the respiratory rate during a normal sleep setting, and owing to its unobtrusiveness and easiness of application, the adhesive-integrated respiration sensor could provide the end users with superior comfort and reliability.

Durability and Biocompatibility of S4 Respiration Sensor: Durability and biocompatibility of the S4 respiration sensor for a long-term recording scenario were tested by applying the sensor to a human user and monitoring the electrical functionality of the sensor along with the conditions of the skin and sensor every 24 h over a 72 h period. During the test, the user carried out daily tasks including 7 h of sleep, 2 showers, 40 min of outdoor cycling, 4 h sitting down, 30 min of walking, 1 h of driving each day. For the entire duration of the test, the sensor's electrical functionality was consistent, indicated by the operation of the LED, and there was no damage to the chip components visually. However, the Tegaderm gradually developed a line of dominant wrinkle created by the repeated folding of the abdomen when the user was sitting down, cycling, and bending down, consequently causing the embedded strain gauge to shift in the direction of Tegaderm's movements (Figure 5d). The semi-permeable characteristics of Tegaderm and spray-on-bandage prevented the build-up of sweat by allowing slow transmission of moisture. These characteristics also successfully insulated the sensor system from water during the shower as well as abrasion from clothing (Figure 5e,f). The part of the skin which had been in contact with polyimide of the S4 did not develop redness or show an indication of irritation, in agreement with previous studies (Figure 5g).[38,39]

Next Steps for S4s: Many components in this report were selected to illustrate the potential for future direction. For example, there already exist variety of packages that are smaller than the chip components presented here. Also, the type of thin-film systems that can be integrated into S4s is virtually limitless. While we used the respiration sensor system to exemplify the benefits of the active, heterogeneous system, it is not hard to imagine that various other surface mount components or thin-film devices compatible with microfabrication processes can be added onto S4s. For example, a part of S4 can be formed into skin-conforming electrodes for biopotential measurements while an on-board pre-amplifier circuit amplifies and filters electrophysiological signals at the source. Long-range wireless communication capabilities can be achieved by implementing a circuit containing a Bluetooth chip, clocks, and a chip antenna. Recent advances in stretchable, skin-conforming far-field radio frequency (RF) antennas also suggest that further improvement in the system's stretchability could be achieved by replacing the chip antenna, which is often the thickest rigid component, with a thin, stretchable antenna.[40,41] Some challenges for achieving fully wireless S4s are the scarcity in small power units with capacity to function as a primary power source as well as the lack of design guidelines for mesh interconnection systems with RF considerations. The use of inductive coils for near-field power transfer has been demonstrated and is an option for S4s for applications requiring intermittent data transfer.[42] For applications demanding a continuous power delivery, emerging far-field energy harvesting technologies enabled by advanced DC rectification and beamforming solutions have potential for allowing continuous health monitoring. Further studies revealing the influence of the serpentine mesh interconnection on the RF characteristic should be conducted to avoid potential parasitic effects or impedance issues in the transmission line. Assigning dedicated planes for ground, power (analog/digital), and signal may be challenging since a mesh is necessarily an array of void features. A potential solution for robust RF performances as well as reliable separation of digital/analog signals may be increasing the density of the mesh, effectively achieving a behavior of solid planes. The effect of the extent of mesh densities on ground effectiveness, impedance control, and noise reduction would need to be investigated. Finally, the packaging method for the completed S4 electronics should not be limited to the lamination of third-party adhesives. Rather, the fabric-based composite substrates presented by Jang et al. or the rapidly curing, extremely skin-compatible elastomer reported by Yu et al. can be considered as exemplar alternative carrier materials depending on the use case.[33,43]

In this report, we introduced a method to fabricate a stretchable, solderable electronic platform and its integration with soft adhesive films for respiration sensing. The S4s proved to be extremely compatible with a standard reflow soldering process using a lead-free solder paste. We further demonstrated the scalability of the method by peeling-off multiple active S4 devices from a secondary donor substrate in a roll format onto a single, large sheet of Tegaderm. Through both mechanical simulation and automatic cyclic tests using the

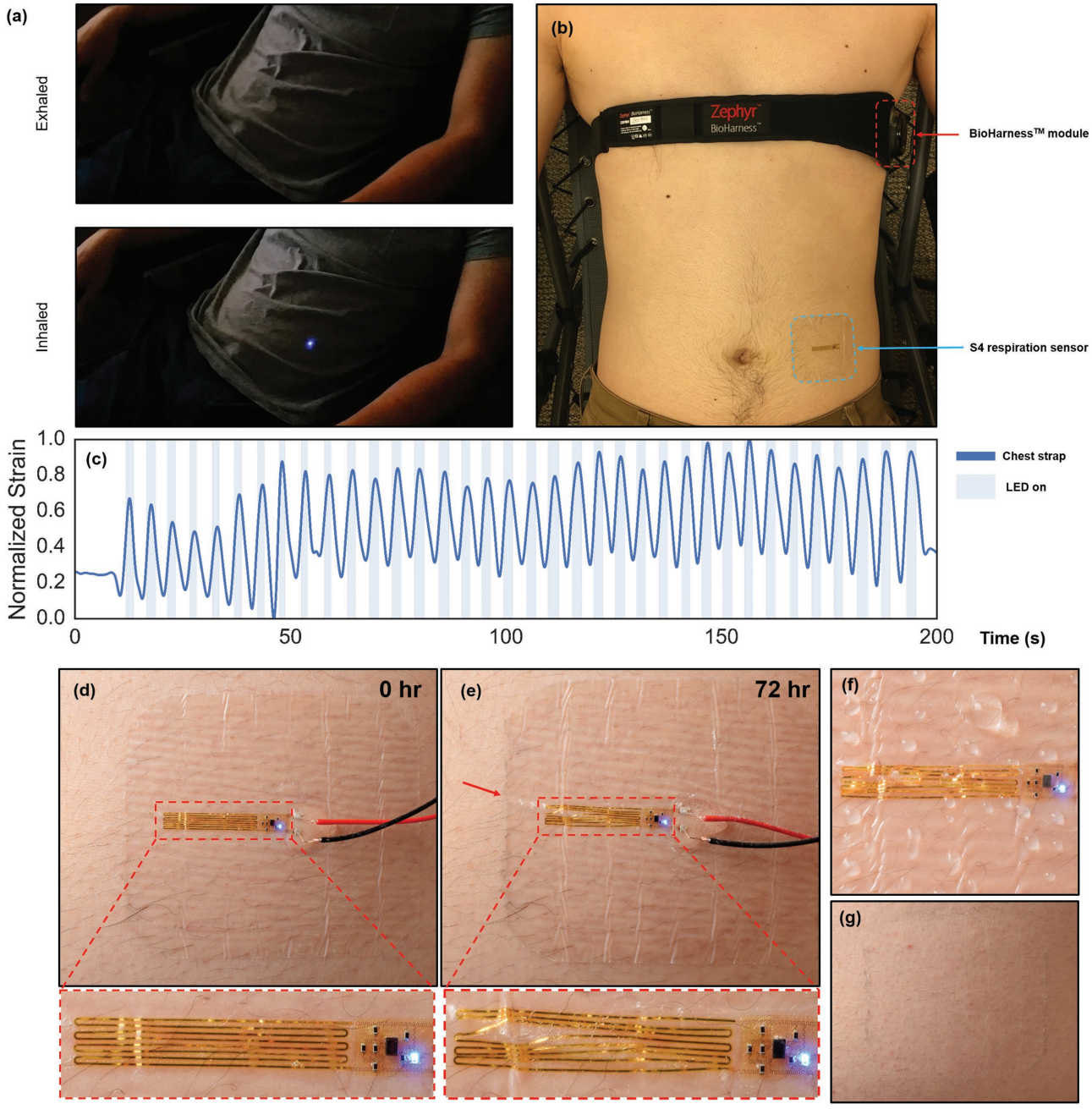

Figure 5. a) Photographs show the "off" (top) and "on" (bottom) states of the S4 respiration sensor. b) Placement of the chest strap and S4 devices. The subject is in a recliner at a near supine position. c) Overlay of the data sets collected by the two devices. Blue curve and shaded light blue areas represent the recorded strain of the chest cavity and the duration of LED indication, respectively, over the 3 min period. Panels (d) and (e) show the photographs of the sensor at the beginning and end of the 72 h period of wear time. The zoom-in insets show the close-up of the S4 respiration sensor. Progressive development of a pronounced wrinkle in the Tegaderm, pointed by the red arrow in panel (e), is observed due to the repeated folding of the abdomen. f) A good protection of the electronics from liquid damage is achieved by Tegaderm and spray-on-bandage. g) 30 min after the removal of the sensor showed no sign of irritation caused by the S4 respiration sensor.

soft pneumatic human surrogate model, we were able to confirm the robustness of the heterogeneous systems embedded in a soft adhesive layer. The presence of Tegaderm helped to relieve localization of stresses in the serpentine interconnects and improved the sensitivity and reliability of the thin film strain gauge. Thus, in addition to providing the clinical benefits, the Tegaderm functioned as the packaging material, stress relief medium, and protective layer for the electronics. The S4 respiration sensor's validity was verified by the simultaneous recording of respiratory rate using the S4 device and a commercial chest strap device. The agreement between the two devices suggests reliable physiological monitoring can be

performed using Tegaderm embedded with an S4. Durability and biocompatibility test results suggest that long-term physiological monitoring can be performed using S4s owing to the mechanical robustness in the interconnection system and Tegaderm's semi-permeable film character.

The manufacturing method presented here intends to bridge what seems to be a wide gap between conventional printed circuit board manufacturing and next-generation stretchable electronics fabrication. The modular nature of constructing S4s and the sheer range of compatible surface mount components available allude to an endless number of future wearable health monitoring applications.

Experimental Section

Strain-Sensitive S4s: To develop a sensor system capable of detecting skin deformation caused by breathing, a Wheatstone bridge and a stage of differential amplifier circuits were incorporated into the S4. A portion of the S4 was directly transformed into a single-element strain gauge made of eight parallel Cr/Au (3 nm/6 nm) traces fully insulated with PI. The resistors used in the remaining Wheatstone bridge arms and the amplification circuit were type 0201 thick film resistors (0.60 mm × 0.30 mm × 0.26 mm, ERJ1G series, Panasonic Electronic Components, USA). The amplification of the voltage offset created by the Wheatstone bridge was done by using a 6-Ball WLCSP amplifier chip with 260 µm solder ball diameter and 400 µm pitch (1.38 mm × 0.91 mm × 0.40 mm, AD8505, Analog Devices, USA). The indicator LED (0.65 mm × 0.35 mm × 0.20 mm, XZBBR155W5MAV, SunLED, USA) was a surface mount chip component with dimensional similarities to 0201 components. The resistance values in the Wheatstone bridge and amplifier circuits were determined by a circuit simulation package (LTspice, Linear Technology Corporation, USA) such that the output of the system was an optical illumination in the presence of strain greater than 1%. The final device configuration of the respiration sensor was completed by connecting a thin lithium polymer battery (3.7 V, 45 mAh, GMB, China) to the power terminals.

Human Surrogate System for Automatic Cyclic Loading Tests: The soft actuator was molded from a platinum cured two-part silicone elastomer (Dragon Skin 20, Smooth-On, USA), and designed following an approach described in recent work on 'Soft Robotics' (Figure S7a, Supporting Information).[44,45] Variable pressure to the actuator was applied via a tube that delivered controlled air flow produced by an Arduino board, a microcontroller, a pump, and solenoid valves, producing a sinusoidal input of 0.27 Hz (16 cpm) to simulate natural respiration rate at rest (Figure S7b, Supporting Information).[46] In order to continuously validate the amount of strain applied to the electronics, two markers for color tracking were attached to the actuator and their movement was recorded with a digital microscope (Dino-Lite, AnMo Electronics Corp., Taiwan). By filtering individual frames of the video with MATLAB and measuring the displacement between the two dots, respective strain for each frame was calculated. The robustness of a Tegaderm-integrated strain gauge was examined throughout the repeated cycles of actuation by attaching the strain gauge to the actuator while placing the remaining circuitry on a rigid surface (Figure S7c, left and Movie S4, Supporting Information). Throughout 3 h of testing, continuous data from the amplifier circuit output, which oscillates due to the cyclic strain applied to the strain gauge, and a video showing the movement of two color markers were recorded. For system-level behavior of an S4 amplifier circuit (Figure S7c, right and Movie S5, Supporting Information), the strain gauge was replaced with an electrical input signal—a 1 Hz sine wave with 0.1 V amplitude. Thus the source of the input oscillation was due to the external sine voltage wave, rather than by the deformation of the strain gauge. Under the same 0.27 Hz actuation frequency, the amplifier output as well as the movement of the color markers was recorded for 3 h. Experiments on human subjects were conducted under approval from Institutional Review Board (IRB) at the University of California San Diego (IRB number: 160127). Informed signed consent was obtained from the subject.

Supporting Information

Supporting Information is available from the Wiley Online Library or from the author.

Acknowledgements

This work was supported in part by the National Science Foundation under Grant IIS-1522125 and the National Institutes of Mental Health under Grant 1R01MH110514. This work was also supported in part by the University of California, San Francisco, California Preterm Birth Initiative, funded by Marc and Lynne Benioff. Microfabrication and assembly were performed in part at the San Diego Nanotechnology Infrastructure (SDNI) of UCSD, a member of the National Nanotechnology Coordinated Infrastructure, which was supported by the National Science Foundation (Grant ECCS-1542148).

Conflict of Interest

The authors declare no conflict of interest.

Keywords

adhesive electronics, reflow soldering, scalable manufacturing, soft robotics, stretchable electronics

Received: March 8, 2017
Revised: May 13, 2017
Published online:

[1] M. E. Berglund, J. Duvall, L. E. Dunne, in *Proc. 2016 ACM Int. Symp. Wearable Comput. – ISWC' 16*, ACM, New York, NY, USA, **2016**, p. 40.
[2] M. H. Iqbal, A. Aydin, O. Brunckhorst, P. Dasgupta, K. Ahmed, *J. R. Soc. Med.* **2016**, *109*, 372.
[3] D.-H. Kim, N. Lu, R. Ma, Y.-S. Kim, R.-H. Kim, S. Wang, J. Wu, S. M. Won, H. Tao, A. Islam, K. J. Yu, T. Kim, R. Chowdhury, M. Ying, L. Xu, M. Li, H.-J. Chung, H. Keum, M. McCormick, P. Liu, Y.-W Zhang, F. G. Omenetto, Y. Huang, T. P. Coleman, J. A. Rogers, *Science* **2011**, *333*, 838.
[4] M. E. Roberts, S. C. B. Mannsfeld, N. Queraltó, C. Reese, J. Locklin, W. Knoll, Z. Bao, *Proc. Natl. Acad. Sci. USA* **2008**, *105*, 12134.
[5] J. Viventi, D.-H. Kim, L. Vigeland, E. S. Frechette, J. A. Blanco, Y.-S. Kim, A. E. Avrin, V. R. Tiruvadi, S.-W. Hwang, A. C. Vanleer, D. F. Wulsin, K. Davis, C. E. Gelber, L. Palmer, J. Van der Spiegel, J. Wu, J. Xiao, Y. Huang, D. Contreras, J. A. Rogers, B. Litt, *Nat. Neurosci.* **2011**, *14*, 1599.
[6] S. Xu, Y. Zhang, L. Jia, K. E. Mathewson, K.-I. Jang, J. Kim, H. Fu, X. Huang, P. Chava, R. Wang, S. Bhole, L. Wang, Y. J. Na, Y. Guan, M. Flavin, Z. Han, Y. Huang, J. A. Rogers, *Science* **2014**, *344*, 70.
[7] T. Sterken, J. Vanfleteren, T. Torfs, M. O. de Beeck, F. Bossuyt, C. Van Hoof, *IEEE Eng. Med. Biol. Soc. Annu. Conf.* **2011**, *2011*, 6886.

[8] W. Gao, S. Emaminejad, H. Y. Y. Nyein, S. Challa, K. Chen, A. Peck, H. M. Fahad, H. Ota, H. Shiraki, D. Kiriya, D.-H. Lien, G. A. Brooks, R. W. Davis, A. Javey, *Nature* **2016**, *529*, 509.
[9] S. Yang, Y.-C. Chen, L. Nicolini, P. Pasupathy, J. Sacks, B. Su, R. Yang, D. Sanchez, Y.-F. Chang, P. Wang, D. Schnyer, D. Neikirk, N. Lu, *Adv. Mater.* **2015**, *27*, 6423.
[10] H.-L. Kao, C. Holz, A. Roseway, A. Calvo, C. Schmandt, in *Proc. 2016 ACM Int. Symp. Wearable Comput. – ISWC' 16*, ACM, New York, NY, USA **2016**, 16.
[11] J. Kim, P. Gutruf, A. M. Chiarelli, S. Y. Heo, K. Cho, Z. Xie, A. Banks, S. Han, K.-I. Jang, J. W. Lee, K.-T. Lee, X. Feng, Y. Huang, M. Fabiani, G. Gratton, U. Paik, J. A. Rogers, *Adv. Funct. Mater.* **2017**, *27*, 1604373.
[12] C. P. Wong, H.-M. Tong, Y.-S. Lai, *Advanced Flip Chip Packaging Springer Science + Business Media*, New York **1999**.
[13] R. Beica, in *Microelectronics Packaging Conference (EMPC)*, IEEE, Piscataway, NJ, USA **2013**, pp. 1–4.
[14] S. Dhivya, V. V. Padma, E. Santhini, *BioMedicine* **2015**, *5*, 24.
[15] S. S. McCord, M. L. Levy, *Semin. Plast. Surg.* **2006**, *20*, 192.
[16] D. Y. Kang, Y.-S. Kim, G. Ornelas, M. Sinha, K. Naidu, T. P. Coleman, *Sensors* **2015**, *15*, 23459.
[17] A. M. Hussain, S. F. Shaikh, M. M. Hussain, *AIP Adv.* **2016**, *6*, 075010; https://doi.org/10.1063/1.4959193.
[18] S.-W. Hwang, H. Tao, D.-H. Kim, H. Cheng, J.-K. Song, E. Rill, M. A. Brenckle, B. Panilaitis, S. M. Won, Y.-S. Kim, Y. M. Song, K. J. Yu, A. Ameen, R. Li, Y. Su, M. Yang, D. L. Kaplan, M. R. Zakin, M. J. Slepian, Y. Huang, F. G. Omenetto, J. A. Rogers, *Science* **2012**, *337*, 1640.
[19] J. Viventi, D.-H. Kim, J. D. Moss, Y.-S. Kim, J. A. Blanco, N. Annetta, A. Hicks, J. Xiao, Y. Huang, D. J. Callans, J. A. Rogers, B. Litt, *Sci. Transl. Med.* **2010**, *2*, 24ra22.
[20] A. Jahanshahi, M. Gonzalez, J. van den Brand, F. Bossuyt, T. Vervust, R. Verplancke, J. Vanfleteren, J. de Beats, *Jpn. J. Appl. Phys.* **2013**, *52*, 05DA18.
[21] D.-H. Kim, Z. Liu, Y.-S. Kim, J. Wu, J. Song, H.-S. Kim, Y. Huang, K.-C. Hwang, Y. Zhang, J. A. Rogers, *Small* **2009**, *5*, 2841.
[22] L. Shen, M. Wang, Y. He, T. F. Lam, Y. Q. Jiang, *Proc. 6th Int. Conf. Electon. Packag. Technol.* **2005**, 419.
[23] X. Deng, G. Piotrowski, J. J. Williams, N. Chawla, *J. Electron. Mater.* **2003**, *32*, 1403.
[24] I. E. Anderson, *J. Mater. Sci.: Mater. Electron.* **2007**, *18*, 55.
[25] C. Yang, S. Lee, J. Wu, T. Lin, *Appl. Surf. Sci.* **2005**, *252*, 1818.
[26] C. A. Harper, *Electronic Assembly Fabrication*, McGraw-Hill, Inc., New York, NY, USA **2002**.
[27] S. M. Won, H. S. Kim, N. Lu, D.-G. Kim, C. D. Solar, T. Duenas, A. Ameen, J. A. Rogers, *IEEE Trans. Electron Devices* **2011**, *58*, 4074.
[28] N. Hu, T. Itoi, T. Akagi, T. Kojima, J. Xue, C. Yan, S. Atobe, H. Fukunaga, W. Yuan, H. Ning, Surina, Y. Liu, Alamusi, *Carbon* **2013**, *51*, 202.
[29] J. Zhou, Y. Gu, P. Fei, W. Mai, Y. Gao, R. Yang, G. Bao, Z. L. Wang, *Nano Lett.* **2008**, *8*, 3035.
[30] M. Romei, A. L. Mauro, M. G. D'Angelo, A. C. Turconi, N. Bresolin, A. Pedotti, A. Aliverti, *Respir. Physiol. Neurobiol.* **2010**, *172*, 184.
[31] K.-J. Chung, C.-F. Lin, W.-C. Chiang, *Trans. Can. Soc. Mech. Eng.* **2012**, *37*, 861.
[32] J. W. Lee, R. Xu, S. Lee, K.-I. Jang, Y. Yang, A. Banks, K. J. Yu, J. Kim, S. Xu, S. Ma, S. W. Jang, P. Won, Y. Li, B. H. Kim, J. Y. Choe, S. Huh, Y. H. Kwon, Y. Huang, U. Paik, J. A. Rogers, *Proc. Natl. Acad. Sci. USA* **2016**, *113*, 6131.
[33] B. Yu, S.-Y. Kang, A. Akthakul, N. Ramadurai, M. Pilkenton, A. Patel, A. Nashat, D. G. Anderson, F. H. Sakamoto, B. A. Gilchrest, R. R. Anderson, R. Langer, *Nat. Mater.* **2016**, *15*, 6.
[34] A. M. Wessendorf, D. J. Newman, *IEEE Trans. Biomed. Eng.* **2012**, *59*, 3432.
[35] A. Aliverti, R. Dellacà, P. Pelosi, D. Chiumello, L. Gattinoni, A. Pedotti, *Ann. Biomed. Eng.* **2001**, *29*, 60.
[36] B. Timmons, J. Salamy, J. Kamiya, D. Girton, *Psychonomic Sci.* **1972**, *27*, 173.
[37] M. A. Sackner, H. F. Gonzalez, G. Jenouri, M. Rodriguez, *Am. Rev. Respir. Dis.* **1984**, *130*, 584.
[38] W.-H. Yeo, Y.-S. Kim, J. Lee, A. Ameen, L. Shi, M. Li, S. Wang, R. Ma, S. H. Jin, Z. Kang, Y. Huang, J. A. Rogers, *Adv. Mater.* **2013**, *25*, 2773.
[39] G. Park, H.-J. Chung, K. Kim, S. A. Lim, J. Kim, Y.-S. Kim, Y. Liu, W.-H. Yeo, R.-H. Kim, S. S. Kim, J.-S. Kim, Y. H. Jung, T.-I. Kim, C. Yee, J. A. Rogers, K.-M. Lee, *Adv. Healthcare Mater.* **2014**, *3*, 515.
[40] A. Haj-Omar, W. L. Thompson, Y.-S. Kim, T. P. Coleman, in *17th Annu. IEEE Wirel. Microw. Technol. Conf. (WAMICON), 2016 IEEE*, IEEE, Piscataway, NJ, USA **2016**, pp. 1–3.
[41] A. Haj-Omar, W. L. Thompson, Y.-S. Kim, P. Glick, M. T. Tolley, T. P. Coleman, in *2016 IEEE Antennas Propag. Soc. Int. Symp. APSURSI 2016 – Proc.*, IEEE, Piscataway, NJ, USA **2016**, pp. 459.
[42] J. Kim, G. A. Salvatore, H. Araki, A. M. Chiarelli, Z. Xie, A. Banks, X. Sheng, Y. Liu, J. W. Lee, K.-I. Jang, S. Y. Heo, K. Cho, H. Luo, B. Zimmerman, J. Kim, L. Yan, X. Feng, S. Xue, M. Fabiani, G. Gratton, Y. Huang, U. Paik, J. A. Rogers, *Sci. Adv.* **2016**, *2*, 8.
[43] K.-I. Jang, S. Y. Han, S. Xu, K. E. Mathewson, Y. Zhang, J.-W. Jeong, G.-T. Kim, R. C. Webb, J. W. Lee, T. J. Dawidczyk, R. H. Kim, Y. M. Song, W.-H. Yeo, S. Kim, H. Cheng, S. Il Rhee, J. Chung, B. Kim, H. U. Chung, D. Lee, Y. Yang, M. Cho, J. G. Gaspar, R. Carbonari, M. Fabiani, G. Gratton, Y. Huang, J. A. Rogers, *Nat. Commun.* **2014**, *5*, 4779.
[44] D. Rus, M. T. Tolley, *Nature* **2015**, *521*, 467.
[45] F. Ilievski, A. D. Mazzeo, R. F. Shepherd, X. Chen, G. M. Whitesides, *Angew. Chem., Int. Ed.* **2011**, *50*, 1890.
[46] X. Zhu, W. Chen, T. Nemoto, Y. Kanemitsu, K. I. Kitamura, K. I. Yamakoshi, D. Wei, *IEEE Trans. Biomed. Eng.* **2006**, *53*, 2553.